



## NW Australian intraplate seismicity and stress regime

S. A. Revets,<sup>1</sup> M. Keep,<sup>1</sup> and B. L. N. Kennett<sup>2</sup>

Received 12 October 2008; revised 18 June 2009; accepted 1 July 2009; published 3 October 2009.

[1] The interrelations between stress orientation, regional deformation, and seismic activity in the context of intraplate seismicity continue to pose difficult questions. Stress models of the Australian continent are largely based on nonseismic information. Our study of 26 microearthquakes in NW Australia shows that they are good indicators of the seismogenic stress field. By inverting focal mechanisms calculated from the events we obtained deviatoric stress tensors in full agreement with the known in-situ stress field. The stress tensors corroborate the elastic modeling of the continent. The methods used here have widespread applicability in determining crustal stress field parameters in regions where in-situ stress data are sparse or absent.

**Citation:** Revets, S. A., M. Keep, and B. L. N. Kennett (2009), NW Australian intraplate seismicity and stress regime, *J. Geophys. Res.*, 114, B10305, doi:10.1029/2008JB006152.

### 1. Introduction

[2] Intraplate seismicity remains a problematic issue in seismology [Stein and Mazzotti, 2007]. The plate tectonic model explains the mechanism of seismic moment release at plate boundaries and predicts that there should be no earthquakes within rigid plates. Studies of continental plates show that in contrast to plate boundaries, deformation within plates is small and slow [Johnston *et al.*, 1994; Stein, 2007]. In contrast to plate boundary earthquakes, there is no model to explain the causes, nature and rate of intraplate earthquakes [Stein, 2007]. One significant handicap is a sparse instrumental record, and concomitant dearth of information of the actual intraplate events [Stein, 2007].

[3] The Australian continent sits on its own plate, the Indo-Australian plate. The continent itself is old and commonly regarded as seismically quiet and stable [Johnston *et al.*, 1994; Leonard *et al.*, 2007]. Tregoning [2003] used GPS data to show that the velocity residuals of 12 stations on the Australian Plate were statistically indistinguishable from zero, with a standard deviation of about 0.6 mm/year. This entails a strain rate smaller than  $6.4 \cdot 10^{-18} s^{-1}$  [Leonard, 2008], a value at the lower end of the spectrum typical for intraplate rates [Mazzotti, 2007]. Tregoning's 2003 conclusion that the Australian continent does not measurably change its dimensions and is thus to all intents and purposes rigid still stands today.

[4] However, intracontinental earthquakes do happen on a regular basis. Leonard [2008] presented a total of 27000 recorded events (with the first record going back to 1788), 17000 of which are considered to be main shocks. The catalogue is reasonably complete for events with magnitude 5.0 and above from 1910 onward and for magnitude 3.5 and

above from 1975 onwards. This database leads to a calculated recurrence rate of 1.1 magnitude 5 or larger events per year, which is similar to the McCue [1990] estimate of a 5 year recurrence of magnitude 6 events. On a regional scale, northwestern Australia has the highest rate for the continent, with a magnitude 5 or larger event every 1.2 years [Leonard *et al.*, 2007].

[5] Western Australia makes up about one third of the continent and is geologically remarkable for containing two Archean cratons: the Yilgarn and Pilbara cratons [Myers *et al.*, 1996] (see Figure 1). The Pilbara Craton in the north is separated by the Paleoproterozoic Capricorn Orogen from the Yilgarn Craton to the south. To the west these two cratons and the intervening Capricorn Orogen are separated from the Indian Ocean by the Neoproterozoic Pinjarra Orogen [Myers *et al.*, 1996] (Figure 1). The Pinjarra Orogen now forms part of a passive margin, a continental remnant of the rift which formed in the Mesozoic with the separation of India from Australia [Myers *et al.*, 1996; Fitzsimons, 2003].

[6] These tectonic elements are separated by various fault systems, including the very large Darling Fault which separates the Pinjarra Orogen over almost its entire extent from the rest of the continent to its east (see Figure 1). The Darling Fault is traceable over more than 1500 km with a downthrow in some places of up to 10 km [Matur, 1974; Dentith and Featherstone, 2003]. The fault has a long and complex history but is currently inactive and aseismic [Harris, 1994]. The tectonic elements themselves also host large numbers of faults, some of which are substantial and extend for hundreds of kilometers [Myers and Hocking, 1998].

[7] Studies of the in-situ stress field of the Australian continent use a variety of stress indicators. Hillis and Reynolds [2003] compiled a database in which focal mechanisms account for just over 7% of the data. Western Australia is described by 58 stress indicators. Only 6 of these are focal mechanisms: 2 from the Canning Basin and 4 from the Perth region.

<sup>1</sup>School of Earth and Environment, University of Western Australia, Crawley, Western Australia, Australia.

<sup>2</sup>Research School of Earth Sciences, Australian National University, Canberra, ACT, Australia.

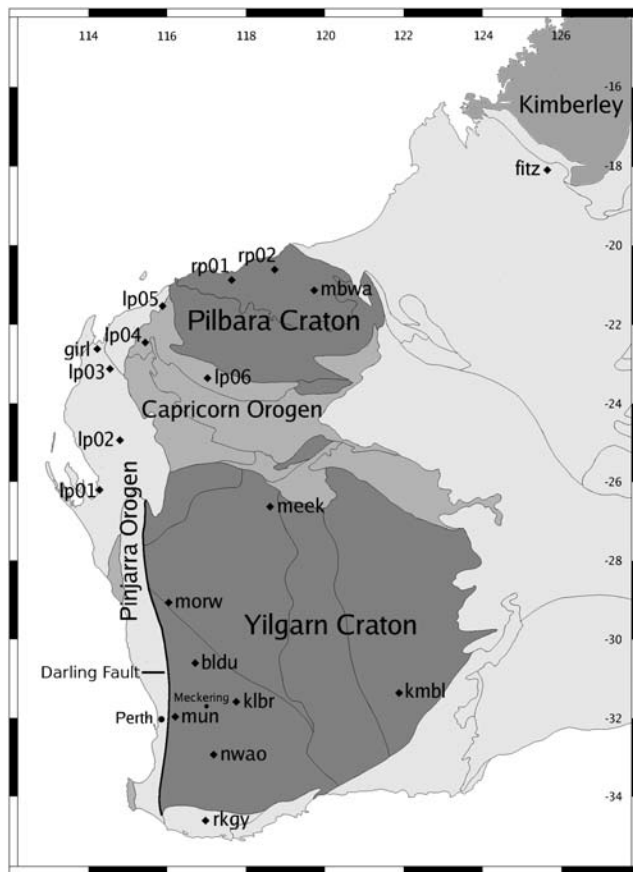


**Figure 1.** Tectonic elements of Western Australia [after Myers and Hocking, 1998] with the location of the stations. For the details of the stations, see Table 1.

[8] Studies of focal mechanisms by Clark and Leonard [2003] and Spassov [1998] were limited to larger events which are necessarily few. For Western Australia, this limitation left 5 events around Meckering in the southwest (about 100 km east of Perth) and 5 events scattered over the Kimberley area in the northeast of the State (see Figure 1).

[9] We present the results of a study of micro earthquakes in NW Australia in which we calculate focal mechanisms and invert these solutions to calculate the deviatoric stress tensor. We compare and contrast our results with stress models of the continent and explore some of the consequences for intraplate seismicity.

## 2. Data and Analysis

### 2.1. Data Acquisition

[10] We deployed a temporary network of eight stations with Guralp CMG-40T seismometers and Reftek 72A-07 recorders along the northwestern margin of Western Australia. The data from these stations was supplemented by data recorded by stations of the Australian National Seismological Network (ANSN) which is managed by Geoscience Australia, as well as from the Global Seismic Network (GSN) stations at Marble Bar and Narrogin (see Figure 1 and Table 1 for the location details of all the stations). We

obtained digital waveforms of the events recorded by the stations of the ANSN through the Data Management Center of the Incorporated Research Institutions for Seismology (IRIS, available online at [www.iris.edu](http://www.iris.edu)).

[11] The eight stations of the temporary network started recording at the end of October 2005. The stations were serviced every six months, and data downloaded from the Reftek disks.

[12] During the 3 year deployment, 28 events occurred in the area between 20° and 30°S and between 112° and 120°E. Two events out of the 28 were too small to be analysed. Initially, we obtained a list of dates and times of events and coordinates of their epicenters from Geoscience Australia, who use the Eqlocl program, developed by the Seismological Research Centre, Victoria [Leonard, 2008]. The events are listed in Table 2 and shown in Figure 2. We used this information to retrieve the waveforms of these events from the data files obtained from our network.

### 2.2. Data Processing

[13] We used the GSAC suite of programs [Herrmann and Ammon, 2007] to process the traces. After identification of the first arrival times of the P and S phase, the trace is cut 5 seconds before and 15 seconds after the P onset.

[14] Digital recorders, including Reftek recorders, apply a number of digital filters to convert the incoming readings from the seismometer to digital data which is then stored on the disk. These Finite Impulse Response filters (FIR) have as a side effect that an incoming impulse is distorted by becoming surrounded, both before and after the pulse, with additional oscillations: the processed signal contains an acausal artifact [Oppenheim and Schaffer, 1999]. This artifact makes it very difficult to read the polarity and the exact time of the P wave arrival accurately. This FIR-induced acausality can be removed by applying an Infinite Impulse Response Filter derived from the FIR filters which caused the artifact [Oppenheim and Schaffer, 1999; Scherbaum, 2001]. We calculated all the necessary IIR filters and used an in-house routine written for the Octave program [Eaton, 2002] which we applied to all the traces to try and ensure a correct reading of the polarity of the first arrival.

**Table 1.** Geographic Position of All Stations

Station	Name	Latitude	Longitude
lp01	Carbla Station	-26.20877	114.28743
lp02	Mooka Station	-24.96491	114.80159
lp03	Winning Station	-23.15305	114.54771
lp04	Nanutarra	-22.48591	115.44500
lp05	Yarraloola Station	-21.56079	115.89007
lp06	Ashburton Downs Station	-23.38715	117.02328
rp01	Sherlock Station	-20.89036	117.63933
rp02	Wallarenya Station	-20.62752	118.72388
bldu	Ballidu (ansn)	-30.61470	116.70910
girl	Giralia (ansn)	-22.64300	114.23400
klbr	Kellerberrin (ansn)	-31.59150	117.75460
kmbi	Kambalda (ansn)	-31.36600	121.88210
mbwa	Marble Bar (gsn)	-21.15897	119.73121
meek	Meekatharra (ansn)	-26.63800	118.61500
morw	Morawa (ansn)	-29.06830	116.03880
mun	Mundaring (ansn)	-31.97830	116.20830
nwao	Narrogin (gsn)	-32.92660	117.23330

**Table 2.** Recorded Regional Earthquakes

Event	Date	Time	Latitude	Error	Longitude	Error	Depth	Error	Magnitude	Location
1	14 Dec 2005	11:02:26	-21.889	0.15	113.701	0.37	21.6	28.1	2.6	W off Exmouth
2	20 Dec 2005	19:49:26	-29.400	0.10	114.102	0.48	10.0	58.7	3.8	SW off Geraldton
3	27 Dec 2005	09:32:05	-24.860	0.17	112.757	0.53	0.0	93.0	3.5	W off Bernier Island
4	29 Jan 2006	09:40:16	-21.676	0.30	113.446	0.50	22.4	61.3	3.4	W off Exmouth
5	5 Feb 2006	20:06:29	-23.737	0.09	114.959	0.14	15.0	51.5	2.6	Middalya Station
6	6 Jun 2006	15:34:09	-25.032	0.05	117.440	0.11	5.5	13.6	4.5	Mount Clere
7	12 Jun 2006	22:43:40	-25.061	0.06	117.556	0.12	1.5	20.1	3.9	Mount Clere
8	2 Sep 2006	15:47:39	-24.433	0.08	116.413	0.13	5.0	35.9	3.5	NW off Landor
9	6 Oct 2006	12:06:04	-22.269	0.11	113.904	0.17	26.1	9.0	3.0	W off Learmonth
10	22 Nov 2006	14:59:43	-25.788	0.09	111.680	0.19	138.7	131.0	2.5	W off Dirk Hartog Island
11	7 Dec 2006	10:58:18	-25.188	0.05	117.411	0.08	14.1	15.5	3.3	SW off Mount Clere
12	10 Dec 2006	16:34:10	-25.085	1.40	117.473	0.20	10.0	184.0	2.7	W off Mount Clere
13	15 Feb 2007	15:38:36	-25.967	0.04	113.276	0.11	18.5	23.4	5.3	Denham Sound
14	30 May 2007	14:31:07	-28.283	0.28	113.822	0.58	0.0	123.0	2.0	Geelvink Channel
15	19 Jun 2007	05:25:18	-20.042	0.56	116.482	0.18	13.6	84.0	2.8	N off Dampier Archipelago
16	28 Jun 2007	16:02:25	-28.741	0.05	112.923	0.10	15.0	20.8	3.2	W off Geraldton
17	17 Jul 2007	10:31:25	-25.535	0.03	113.319	0.07	0.0	16.5	2.6	N off Perron Peninsula
18	26 Aug 2007	00:34:34	-22.145	0.13	115.369	0.10	5.7	25.0	3.2	W off Mount Minnie
19	15 Sep 2007	04:01:10	-28.430	0.03	113.824	0.07	16.6	14.0	2.2	E off Wallabi Islands
20	25 Oct 2007	01:28:14	-23.774	0.08	114.667	0.19	18.7	30.2	3.5	W off Gooch Range
21	4 Nov 2007	12:19:52	-23.842	0.08	114.861	0.16	15.0	32.9	4.0	Middalya Station
22	7 Nov 2007	19:10:45	-23.833	0.06	114.933	0.12	0.0	26.5	4.4	Middalya Station
23	27 Nov 2007	02:48:16	-23.219	0.09	115.047	0.11	10.0	20.7	3.7	Towera Station
24	13 Jan 2008	16:16:58	-26.650	0.11	117.069	0.11	2.5	34.2	2.9	W off Meekatharra
25	15 Jan 2008	12:51:52	-29.990	0.13	115.739	0.32	10.0	31.7	2.3	E off Eneabba
26	28 Jan 2008	15:37:13	-22.683	0.18	113.872	0.14	7.2	19.0	3.1	SW off Learmonth
27	18 Feb 2008	19:18:55	-26.693	0.31	112.770	0.89	10.0	164.9	2.8	W off Tamala Station
28	31 Mar 2008	08:27:48	-27.666	0.06	112.332	0.17	17.7	25.0	4.4	W off Kalbarri

[15] We processed arrival times and polarity with the HYPOELLIPSE program [Lahr, 1999] to relocate the hypocenters, using the preliminary crustal velocity models shown in Table 3. These crustal models are highly simplified versions of initial results of inversion from receiver function studies at the stations of our network.

[16] The relocated hypocenters mostly fell within the margin of error of the Geoscience Australia calculations (Table 2).

[17] HYPOELLIPSE also generates the necessary data input files for the FPFIT program [Reasenber and Oppenheimer, 1985] which we used to calculate the focal mechanisms.

### 2.3. Stress Tensor Inversion

[18] We used the focal mechanism stress inversion method proposed by Gephart and Forsyth [1984] and Gephart [1990a] to estimate the deviatoric stress tensor from the nodal planes of the focal mechanism. Gephart [1990b] demonstrated how the method is based on minimizing the smallest angle between the observed fault geometry and any fault geometry consistent with the principal stress directions.

[19] Each of the fault planes is described by a Cartesian coordinate set, with  $x'_1$  the direction of the fault plane pole,  $x'_2$  the B axis direction (the direction parallel with the intersection of the two nodal planes) and  $x'_3$  the slip direction, and the regional stress by the directions of the main stress components. The relation of stress tensor components between these two coordinate systems is

$$\sigma'_{ij} = \sigma_{kl} \beta_{ik} \beta_{jl} \quad (1)$$

The maximum shear stress and mean normal stress are respectively

$$\tau_m = \frac{\sigma_1 - \sigma_3}{2}, \quad \sigma_m = \frac{\sigma_1 + \sigma_3}{2} \quad (2)$$

The absolute values of the stress tensor are inaccessible, but the relative magnitudes of the principal stress components can be calculated. Their relation is given by

$$R = \frac{\sigma_2 - \sigma_1}{\sigma_3 - \sigma_1} \quad (3)$$

The three normalized stress components acting on a fault plane can now be described as

$$\sigma = \frac{\sigma'_{11} - \sigma_m}{\tau_m}, \quad \tau_b = \frac{\sigma'_{12}}{\tau_m}, \quad \tau_s = \frac{\sigma'_{13}}{\tau_m} \quad (4)$$

and are completely determined by the dimensionless quantities  $R$  and  $\beta_{ij}$ . The shear stress will match the slip direction on a plane when  $\sigma'_{12}$  is zero, which implies that

$$R = \frac{\sigma_2 - \sigma_1}{\sigma_3 - \sigma_1} = -\frac{\beta_{13}\beta_{23}}{\beta_{12}\beta_{22}} \quad (5)$$

[20] Most combinations of fault orientation and stress model will fail to fulfill this condition ( $\sigma_{12} = 0$ ) and a misfit criterium can be chosen to help and minimize the misfit between model and data. To do so, Gephart and

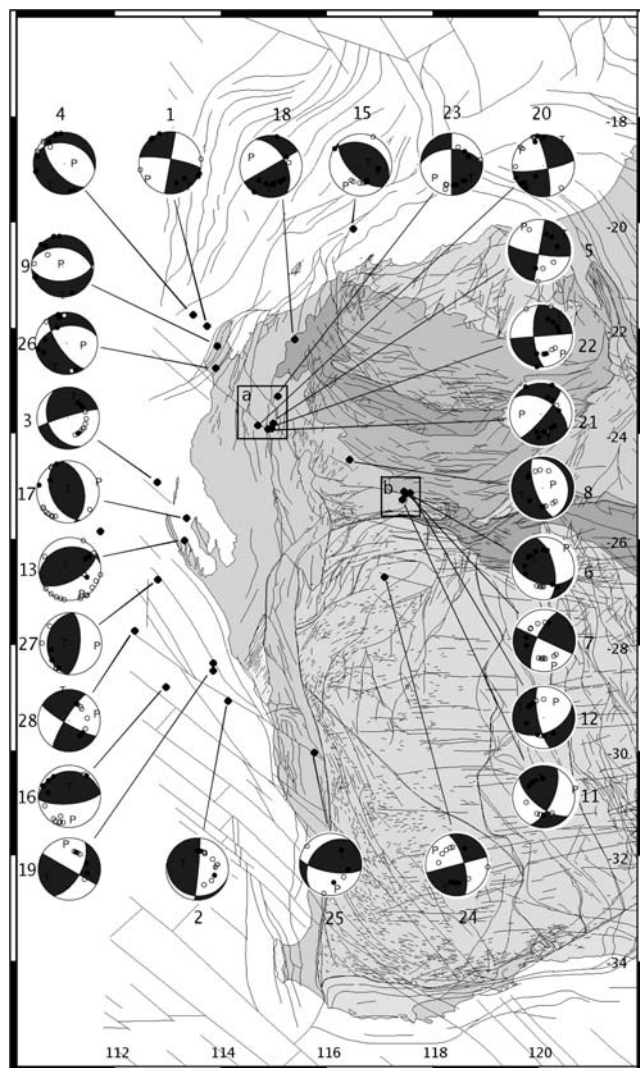


**Figure 2.** Geological map of Western Australia with mapped faults superimposed [after *Myers and Hocking, 1998*] and with the results of the focal mechanism calculations. The events are numbered in chronological order, with details in Table 2. The rectangles are group clusters of events: (a) the Middalya group and (b) the Mount Clere group.

*Forsyth* [1984] proposed to minimize the rotation matrix  $\alpha$  defined as

$$\beta'_{ij} = \alpha_{ik} \beta_{kj} \quad (6)$$

and requiring that

$$R = -\frac{\beta'_{13}\beta'_{23}}{\beta'_{12}\beta'_{22}} \quad (7)$$

A grid search over the parameter space with a one-norm misfit (using the absolute deviate rather than the traditional two-norm squared deviate) yields then the required values of the deviatoric stress tensor (problems with the statistics of the one-norm used by *Gephart* and identified by *Hardebeck and Hauksson* [2001] have been resolved [Revets, 2009].

[21] The calculated parameters can be used to construct an unscaled Mohr circle [*Jaeger and Cook, 1979*], on which the poles of the fault planes can be plotted, following the procedure given by *Zizicas* [1955]. *Gephart* [1990b] advocated a modification of this methodology and proposed a Mohr sphere, using the three stress components as defined in equation (4). The Mohr circle in common usage is the projection of this Mohr sphere on the  $\sigma, \tau_s$  plane for which  $\tau_b$  is zero.

[22] Geometrically possible fault geometries are presented within the volume between the largest sphere and the two smaller ones. Slip is most likely on planes subject to high shear stress ( $\tau_s$ ) and low normal stress ( $\sigma$ ): fault planes should therefore plot in the upper and lower left part of a  $\tau_s, \sigma$  graph. Fault planes with a negative  $\tau_s$  move against the shear stress direction and are therefore misoriented by  $180^\circ$ .

[23] The shear stress should match the slip direction for failure, which was formalized in equation (5). Therefore actual fault planes should plot on or very close to the  $\tau_b$  zero axis.

[24] Thus plotting the poles of the actual fault planes on an unscaled Mohr sphere defined by the deviatoric stress tensor shows how consistent the fault planes are with the stress tensor.

### 3. Results

#### 3.1. Focal Mechanisms

[25] The epicenters of the events lie in the vicinity of significant faults mapped by the Geological Survey of Western Australia (see Figure 2) [after *Myers and Hocking, 1998*]. As the confidence limits of the calculated position of the epicenters are usually between 10 and 20 km and those of the depth at least as large (see Table 2), hypocenters may well coincide with known faults. The events studied here are small and occur at depth, and verification of location on the ground is impossible, a common occurrence for most Australian earthquakes [*Clark and McCue, 2003*]. Because the events are small and because of the error margins on the hypocenter locations, the actual earthquake may have happened on adjacent zones of weakness, rather than on the larger known faults.

[26] The calculations to remove the acausality effects of the decimation process during acquisition of the traces on the first arrival appear to be highly effective. Out of a total of 306 polarities used to calculate the various focal mechanisms, 14 proved to be discrepant and this despite the fact

**Table 3.** Preliminary Crustal Velocity Models Used for Hypocenter Relocation

Region	Depth (km)	$v_P$	$v_P/v_S$
Yilgarn	00.0	6.23	1.73
	19.0	6.95	1.73
	36.0	8.27	1.73
Pilbara	00.0	6.23	1.73
	28.0	8.27	1.73
Pinjarra	00.0	6.23	1.71
	15.0	6.95	1.71
	30.0	8.27	1.71
Capricorn	00.0	6.23	1.75
	33.0	8.27	1.75

**Table 4.** Focal Mechanisms and Stress Tensor Fit<sup>a</sup>

Event	Nodal Plane		N	D	Uncertainty		SDR	Misfit	Rotated Plane 1		Rotated Plane 2		Slip Index			
	#	Azimuth			Dip	Strike			Dip	Azimuth	Dip	Azimuth			Dip	
1	1	10.0	90.0	10	0	10	20	0.83	0.00	10.0	90.0	280.0	80.0	+	-	*
1	2	280.0	80.0						43.30	280.0	36.7	190.0	90.0	+	-	*
2	1	5.0	87.2	14	2	3	10	0.56	4.10	8.9	86.1	113.6	15.3	-	-	
2	2	105.6	15.0						38.36	100.0	53.3	6.3	85.1	-	-	*
3	1	154.7	35.0	13	1	8	40	0.78	12.72	144.3	25.7	245.5	84.7	+	+	
3	2	253.1	84.1						6.63	258.1	83.3	159.8	38.8	+	+	
4	1	140.1	59.8	12	0	10	13	0.46	33.82	100.0	53.3	284.2	36.8	+	-	*
4	2	283.8	35.8						2.42	280.0	36.7	139.9	60.2	+	+	*
5	1	10.0	90.0	8	0	3	13	0.60	0.00	10.0	90.0	100.0	80.0	+	+	*
5	2	100.0	80.0						26.70	100.0	53.3	190.0	90.0	+	+	*
6	1	104.9	49.9	14	0	8	0	0.51	5.11	100.1	53.3	346.3	61.6	-	-	*
6	2	347.1	60.9						27.66	9.7	56.1	138.1	47.2	-	-	
7	1	205.0	70.0	14	0	3	8	0.61	24.81	190.0	90.0	280.0	87.3	+	+	*
7	2	295.0	90.0						38.44	91.7	59.3	200.4	61.7	+	-	
8	1	160.0	70.0	12	0	0	0	0.50	35.53	190.0	90.0	280.0	5.4	+	-	*
8	2	340.0	20.0						31.17	280.0	36.7	160.1	69.6	+	+	*
9	1	85.0	50.0	10	0	13	13	0.66	11.42	100.0	49.1	280.8	41.0	+	+	
9	2	280.0	41.0						1.73	282.4	40.3	85.5	50.9	+	+	
11	1	25.1	64.9	11	0	5	3	0.54	8.49	27.7	65.3	135.3	56.7	-	-	
11	2	128.9	63.0						2.45	127.6	64.5	25.6	66.4	-	-	
12	1	65.0	50.0	12	1	3	0	0.40	27.47	100.0	53.3	8.6	88.1	+	-	*
12	2	168.0	75.0						26.42	190.0	90.0	100.0	45.3	+	-	*
13	1	60.0	60.2	20	1	5	5	0.60	33.44	98.9	58.8	254.6	33.6	-	-	
13	2	258.9	31.2						0.04	258.9	31.2	60.0	60.2	-	-	
15	1	135.0	60.2	10	0	8	5	0.56	29.40	100.8	58.5	299.6	32.9	-	-	
15	2	296.1	31.2						0.07	296.1	31.1	135.0	60.3	-	-	
16	1	85.0	70.0	13	0	3	10	0.53	12.79	98.3	70.2	257.9	21.0	-	-	
16	2	265.0	20.0						2.17	260.4	21.0	86.1	69.1	-	-	
17	1	19.3	35.9	13	1	3	8	0.62	53.62	280.0	36.7	139.1	60.0	+	-	*
17	2	139.9	69.8						38.40	100.0	53.3	343.5	59.1	+	-	*
18	1	60.0	90.0	12	0	8	8	0.72	37.22	213.0	64.2	323.0	54.7	+	-	
18	2	330.0	50.0						7.34	324.3	55.4	55.1	88.8	+	+	
19	1	30.0	60.0	8	1	8	15	0.59	35.53	190.0	90.0	100.0	84.6	-	-	*
19	2	300.0	90.0						41.11	100.0	53.3	355.6	71.5	-	+	*
20	1	79.9	80.0	14	1	0	5	0.64	31.12	88.2	50.6	354.1	85.1	+	+	
20	2	348.1	80.0						0.20	348.2	79.8	80.0	79.9	+	+	
21	1	40.1	80.1	14	1	3	5	0.65	29.05	198.2	80.8	295.1	53.1	+	-	
21	2	301.9	51.0						7.24	307.0	44.9	44.6	82.5	+	+	
22	1	85.0	90.0	14	2	3	10	0.70	23.93	71.9	77.8	171.1	53.5	-	-	
22	2	175.0	70.0						24.64	7.3	88.5	97.3	86.8	-	+	
23	1	180.0	90.0	12	0	0	0	0.54	9.99	190.0	90.0	280.0	50.0	-	+	*
23	2	270.0	50.0						14.93	280.0	36.7	184.1	85.6	-	+	*
24	1	75.0	90.0	12	0	10	20	0.71	43.39	99.8	53.2	352.0	67.9	+	+	
24	2	345.0	70.0						2.49	343.5	71.9	253.4	89.8	+	-	
25	1	100.1	69.8	6	1	13	10	0.73	6.17	94.0	67.7	220.9	34.3	-	-	
25	2	220.7	35.9						25.29	239.3	16.1	83.1	75.2	-	-	
26	1	145.0	70.0	11	2	10	10	0.53	42.48	100.5	51.7	252.2	41.9	+	+	
26	2	257.1	44.0						2.17	259.0	45.7	146.7	68.8	+	+	
27	1	5.0	65.0	7	0	10	3	0.38	5.91	359.4	67.7	182.6	22.3	-	-	
27	2	185.0	25.0						31.62	227.4	45.5	9.1	51.4	-	-	
28	1	120.1	80.0	10	0	0	5	0.47	31.13	112.3	50.6	206.0	85.5	+	+	
28	2	211.9	80.0						0.20	211.8	79.8	120.0	79.9	+	+	

<sup>a</sup>For each event, the nodal plane (#) is described by its azimuth and dip, followed by the number of stations (N), number of discrepant polarities (D) as well as the 90% uncertainty on strike and dip and the Station Distribution Ratio (SDR). These are followed by the results of the stress tensor calculations for all focal mechanisms taken together. For each nodal plane, the angular misfit, required rotation of nodal plane and its relative auxiliary in azimuth and dip are shown, as well as the initial direction of slip and the direction of slip after rotation. An asterisk indicates that the shear stress is very low and unlikely to cause failure.

that we are dealing with micro earthquakes recorded at significant distances (see column N and D in Table 4).

[27] About two thirds of the focal mechanisms show a significant strike-slip component to displacement, with the other third predominantly either normal or reverse faults, and a single pure dip-slip (event 2) faulting event (Figure 2). The average uncertainty on the calculated strike is  $5.8^\circ$  (standard deviation  $4.1^\circ$ ) while that of the calculated dip is

$9.2^\circ$  (standard deviation  $8.4^\circ$ ). The orientation and the values of the 90% confidence intervals of the nodal planes are listed in Table 4. FPFIT also calculates a Station Distribution Ratio (SDR in Table 4). It is a measure (between zero and one) of the distribution of the data points on the focal sphere relative to the radiation pattern. This number becomes smaller as more and more data points lie nearer the nodal planes. This particular weighing reflects the

**Table 5.** Stress Tensor Parameters<sup>a</sup>

Scope	$n$	Misfit	$R$	$\Phi$	$\sigma_1$		$\sigma_2$		$\sigma_3$		CI
					Plunge	Azimuth	Plunge	Azimuth	Plunge	Azimuth	
All FPS	26	9.51	0.31	53.3	0	100	53	190	37	10	4.9
Capricorn	11	10.25	0.36	-14.0	15	95	13	1	69	231	8.8
Pinjarra	14	7.66	0.30	53.2	0	99	53	189	37	9	5.7
Cape Range	9	6.01	0.24	55.0	0	100	55	190	35	10	6.0
Middalya	6	2.68	0.80	85.5	85	92	5	268	0	1	3.7
Mount Clere	5	4.36	0.44	4.8	56	113	3	207	34	298	7.1
Abrolhos	9	3.63	0.49	-12.1	30	125	10	29	58	282	3.4

<sup>a</sup>Stress tensor inversions for various sets of focal mechanisms are listed, with  $n$  indicating the number of events included, followed by the average minimum angular misfit,  $R$ , indicating the relative sizes of the stress components,  $\Phi$ , which fixes the orientation of  $\sigma_2$  and  $\sigma_3$  in plane perpendicular to  $\sigma_1$ , then the plunge and azimuth of each stress component and finally the 95% confidence interval on the component directions.

fact that determining the polarity from observations near nodal planes is more difficult and inconsistencies more prevalent. *Reasenber and Oppenheimer* [1985] drew particular attention to this measure as a guide to critical assessment of the calculated solutions. Solutions with a SDR smaller than half are less robust than those with higher SDR values, and may well have to be rejected. *Kilb and Hardebeck* [2006] explored and discussed the implications of this measure in great detail. They concluded from an analysis of the Northern California Earthquake Data Center catalog that an SDR of at least 0.58 is necessary to achieve 60% consistency of the focal mechanisms. In our set of events, half of the focal mechanisms meet this threshold, with a further 6 achieving a SDR above 0.50.

### 3.2. Stress Tensor Inversion

[28] Inversion of the nodal plane orientations from all the focal mechanisms yields stress orientations from the deviatoric stress tensor which are broadly consistent with published results (Table 5). These studies, also based on focal mechanisms [*Leonard et al.*, 2002; *Clark and Leonard*, 2003; *Spassov*, 1998] were for Western Australia limited to the Perth area. The orientations we obtain are consistent with the proposed stress model of the entire continent [*Hillis and Reynolds*, 2003].

[29] The result of this first calculation using all focal mechanisms is shown in Table 4. The average minimum angular misfit of about  $9.5^\circ$  is somewhat high, which raises the question of possible heterogeneity of the data set. A Kolmogorov-Smirnov test of normality of all the misfit values yields a probability of 0.06. This probability increases to 0.49 when the 6 outliers, clearly visible in a histogram of the rotation misfits (Figure 3), are removed. There is no correlation between magnitude of an event and the misfit to the modeled stress tensor ( $r = -0.12$ ). Identification of the outliers shows that most refer to events in the Capricorn Orogen.

[30] A plot of the fault plane positions on the Mohr sphere shows that a significant number of the planes are unlikely to fail under the stress regime defined by the stress tensor obtained from all the focal mechanisms (Figure 4). The number of planes for which  $\tau_b$  is clearly different from zero as well as the number of planes with a negative  $\tau_s$  invites further scrutiny. Identifying these planes reinforces the earlier indication that the Capricorn Orogen events differ from the other events. We performed a series of inversions

using subsets of the focal mechanism solutions, choosing groups on the basis of the tectonic element in which or along which they happened. Table 6 lists the events included in the various groups.

#### 3.2.1. Capricorn Orogen Stress Tensor

[31] Inspection of the events which are outliers with regard to the minimum angular misfit or with slip in the opposite direction of the modeled one using all events shows that most of these belong to the Capricorn Orogen group of events and in particular the Mount Clere cluster (see Figure 2, rectangle b). Event 24 is the only event recorded in the Yilgarn Craton, but it is included in this group as it is well away from the Pinjarra Orogen.

[32] Inversion using this subset of the focal mechanisms yielded a slightly worse fit than the inversion using all events, with the average rotational misfit climbing to  $10.25^\circ$  for 11 events (see Table 5 and Figure 5). The Mohr sphere plots show an increased scatter of the fault planes with even more fault planes either unlikely to fail or slipping in the opposite direction of the modeled one. This failure to improve the fit of the data to a modeled stress tensor could be an indication that the events reflect local conditions whereby stress failure orientation is modified by near surface effects rather than reflect the larger-scale seismogenic, deep crustal stress field.

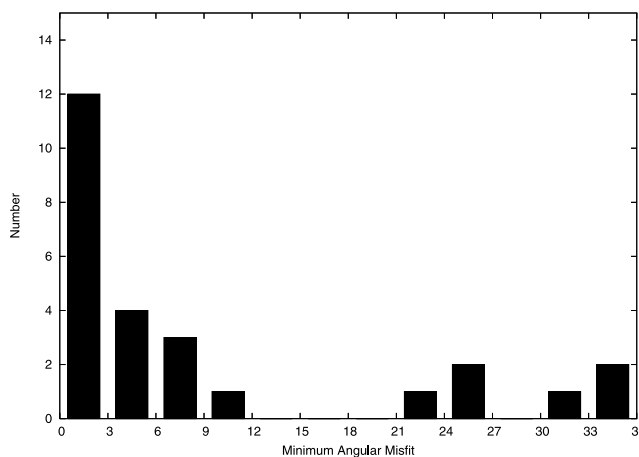


**Figure 3.** Histogram of the minimum angular misfit of the stress tensor inversion using all events.

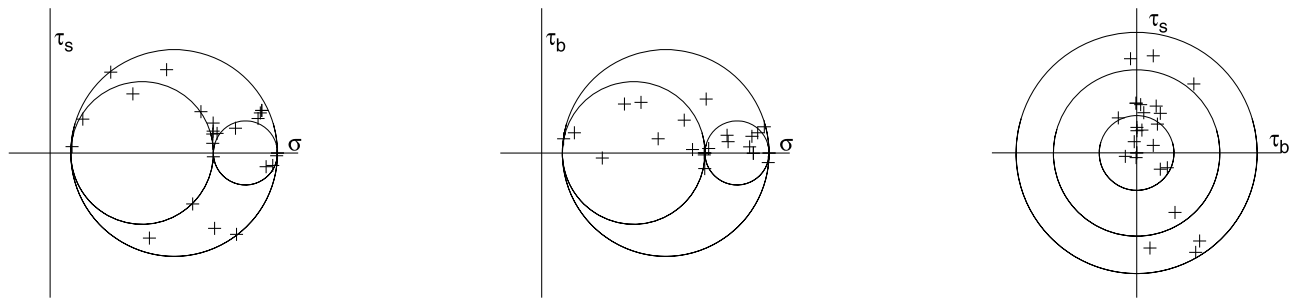


**Figure 4.** Mohr sphere projections showing the poles of all the fault planes relative to the stress components defined by the stress tensor obtained from inverting all focal mechanisms.

[33] The Capricorn group of events is made up of two clusters: the Middalya cluster on boundary between the Capricorn and Pinjarra Orogen (Figure 2, rectangle a) and the Mount Clere cluster, some 40 km north of the boundary between the Capricorn Orogen and the Yilgarn Craton (Figure 2, rectangle b). If local heterogeneities control the failure geometry of the smaller events, scatter of the fault planes on the Mohr sphere should continue to be large.

[34] Separate stress tensor inversion for the two clusters shows a continuation of heterogeneity for the Mount Clere cluster, but not for the Middalya cluster (see Table 5). There are significant changes to the stress tensors. The azimuth of  $\sigma_1$  remains broadly similar to that calculated for the other groups, but both plunge of  $\sigma_1$  and the shape of the tensor (described by  $R$ ) change significantly. In case of the Mount Clere cluster,  $\sigma_1$  plunges  $56^\circ$  while the shape of the tensor shows a decrease in axial compression as  $R$  increases to 0.44. In case of the Middalya cluster,  $\sigma_1$  is almost vertical with its plunge of  $85^\circ$  and the shape of the tensor has changed completely and now represents axial extension with  $R$  at 0.80 (Table 5).

### 3.2.2. Pinjarra Orogen Stress Tensor

[35] The stress tensor inverted from the focal mechanisms of the Pinjarra Orogen events is indistinguishable from the one calculated from all the events taken together (Table 5). This demonstrates that the one-norm misfit criterion used by the inversion method of *Gephart* [1990a] is highly effective in dealing with heterogeneous data. It also supports the separation of the Capricorn group of events. Inspection of the Mohr sphere projections (Figure 6) of the calculated fault planes versus the stress tensor shows an excellent fit, with just two anomalous events (17 and 19). This is a remarkable result, as the events included in this group span some 1000 km, and heterogeneity at such a scale is very likely, particularly for such small events. The absence of any correlation between magnitude of an event and the misfit to the modeled stress tensor ( $r = -0.11$ ) further supports the reliability of using such small events.

[36] In parallel with the approach to the nature of the stress tensor in the Capricorn Orogen, we broke up the events in the Pinjarra Orogen into two smaller geographic groups (Cape Range group and Abrolhos group as shown in Table 6). The stress tensors calculated for these groups confirm the suggested stress homogeneity (Table 5). The Cape Range tensor is very similar to the Pinjarra Orogen tensor as well as to the tensor calculated from all events.

The tensor calculated from the Abrolhos group of events differs somewhat from the others, with an azimuth  $125^\circ$  and a plunge of  $30^\circ$  for  $\sigma_1$  and with a tensor shape exactly between tensional and compressional ( $R = 0.5$ ).

[37] The  $\sigma_1$  component of the Abrolhos stress tensor aligns very well with the many transfer faults west of the continent (see Figure 2). The Abrolhos group differs from the other groups as about half of the events occur under the continental rise and hence close to the outer edge of the continent.

[38] The two events with substantial misfit against the Pinjarra tensor (17 and 19) fall much better into place in the modeled Abrolhos tensor, while event 17 remains a substantial misfit to the Cape Range tensor.

### 3.3. Stress Regime in Context

[39] The orientation of the overall stress tensor is consistent with the measurements and modeling of the stress on the Australian continent [*Hillis and Reynolds*, 2003; *Reynolds et al.*, 2002, 2003]. Adding the directions of the main stress component from our calculations (black arrows) to the stress map of Australia yields Figure 7, with the white arrows showing the orientation of the calculated main stress of the various stress provinces by *Hillis and Reynolds* [2003]. The maximum horizontal stress component of the stress tensor for the Pinjarra Orogen (PO), Capricorn Orogen (CO), as well as those of the subgroups Cape Range (CR), Middalya (Mi) are indistinguishable from the *Hillis and Reynolds* results. The orientation of the maximum horizontal stress from the tensor of the Mount Clere group is slightly different and trending more ESE, while the orientation from the Abrolhos subgroup tensor is significantly different and trends in an almost SE direction. Nevertheless, both are broadly aligned with the overall stress tensor.

[40] *Burbidge* [2004] proposed an alternative model, using the thin plate spherical finite element modeling

**Table 6.** List of Events Included in Geographic Subgroups

Scope	Included Events
Capricorn	5, 6, 7, 8, 11, 12, 20, 21, 22, 23, 24
Pinjarra	1, 2, 3, 4, 9, 13, 16, 17, 19, 20, 25, 26, 27, 28
Cape Range	1, 3, 4, 9, 13, 15, 17, 18, 26
Middalya	5, 8, 20, 21, 22, 23
Mount Clere	6, 7, 8, 11, 12
Abrolhos	2, 3, 13, 16, 17, 19, 25, 27, 28

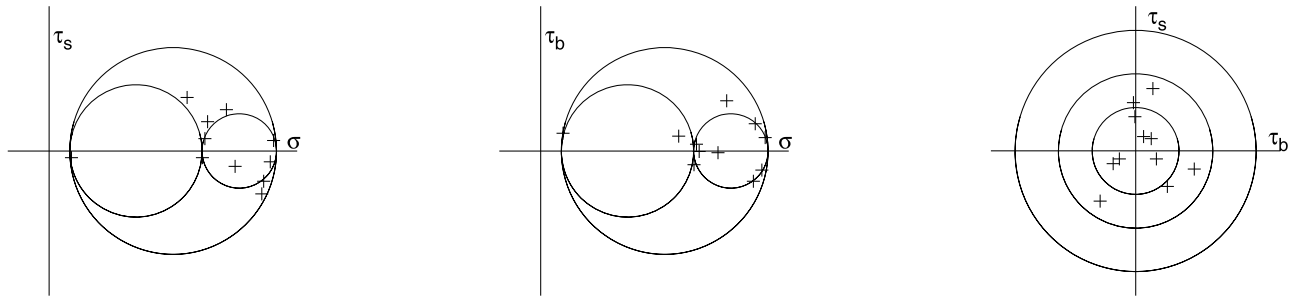


**Figure 5.** Mohr sphere projections showing the poles of the fault planes of the events in the Capricorn Orogen relative to the stress components defined by the stress tensor obtained from inverting the focal mechanisms of the Capricorn Orogen events.

technique, in contrast to the previous elastic models [Coblentz *et al.*, 1998; Reynolds *et al.*, 2002]. His best fitting model predicts maximum horizontal principal stress directions along the southern half of the Western Australian coast more or less parallel with the coast. The model also predicts that thrust faulting will be the dominant mode of faulting for most of the western three quarters of the continent. The orientation of the stress tensors and the focal mechanisms calculated in this study do not fulfill these predictions.

#### 4. Discussion

[41] Two thirds of the events used for stress tensor inversion occurred at depths at or below 10 km. The uncertainties on the depth estimates of the hypocenters are substantial (see Table 2). Our attempts at relocation of the events by incorporating the arrival times recorded by our temporary network to the arrival times recorded by the permanent network yielded broadly similar hypocentral depths, which leads us to regard the calculated hypocentral depths as acceptable. These hypocentral depths indicate that the stress regime sampled is that of the seismogenic crust rather than the result of stress reorientation by near surface features. Our data set extends well below that accessible to quarrying activities or normal drilling operations. The consistency between stress directions derived largely from shallower sources of data [Hillis and Reynolds, 2003] and our data set supports the suitability of micro earthquakes as

a useful source of information for the determination of the crustal stress field.

[42] The absence of correlation between magnitude or depth of events with minimum angular misfit between fault plane and modeled stress tensor indicates that the micro earthquakes studied are sufficiently unbiased with regard to local effects to be useful for stress inversion. These correlations are absent for all the groups of events, even when subgroups yielded somewhat different stress tensors.

[43] Sandiford and Egholm [2008] highlighted that the Darling Fault, a steep ( $70^\circ$ ) west dipping, north-trending structure, has no historical record of seismicity, despite being misoriented by only a few 10s of degrees for failure in reverse fault mode. As shown here,  $\sigma_1$  of the Abrolhos stress tensor has a plunge of  $30^\circ$ , making it virtually normal to the plane of the Darling Fault. This combination of orientations is sufficient to explain seismic quiescence of the Darling Fault as first suggested by Dentith and Featherstone [2003]: the stress on the Darling Fault effectively locks it into place.

#### 5. Conclusions

[44] Micro earthquakes can be used, even with a modest recording network, to calculate focal mechanisms reliably when care is taken with the assessment of first arrival polarity. The deconvolution of the FIR induced acausality from the traces proves to be highly effective.

[45] Focal mechanisms from micro earthquakes can be used to calculate (deviatoric) stress tensors and provide

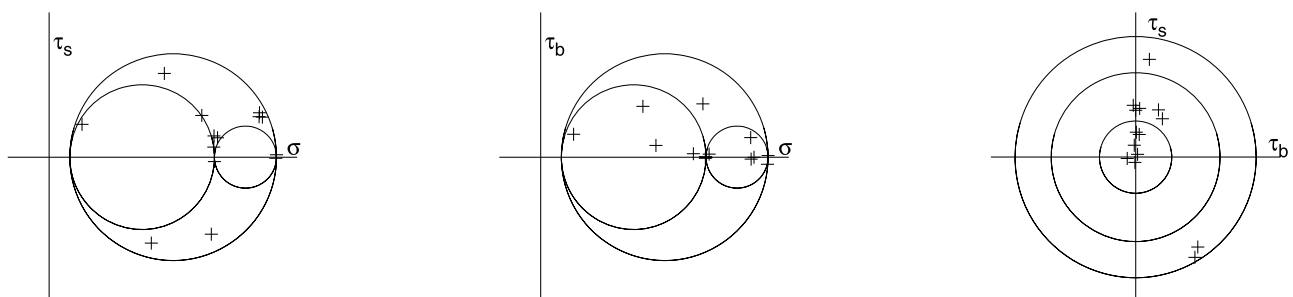


**Figure 6.** Mohr sphere projections showing the poles of the fault planes of the events in the Pinjarra Orogen relative to the stress components defined by the stress tensor obtained from inverting the focal mechanisms of the Pinjarra Orogen events.

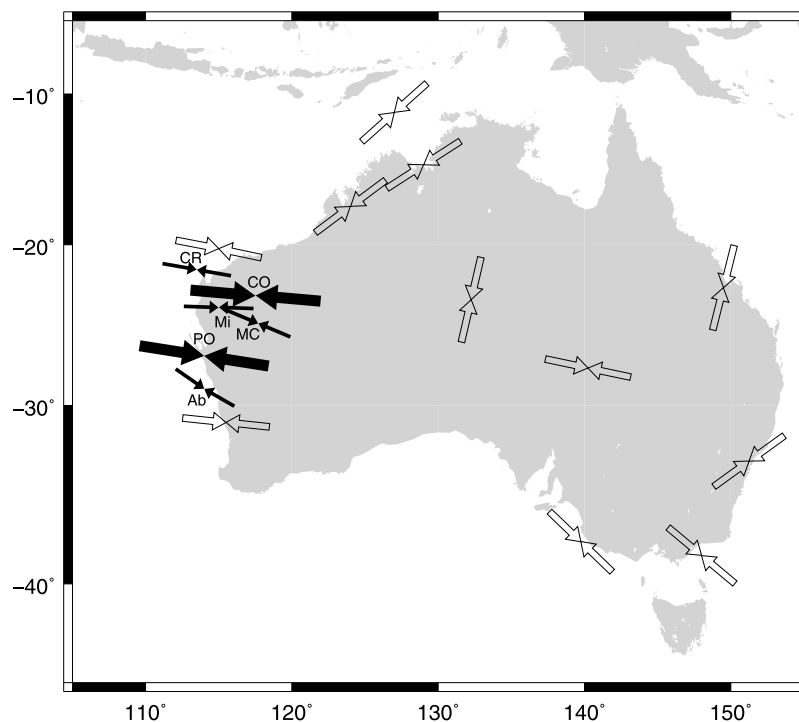


**Figure 7.** Summary map with  $\sigma_1$  stress directions from our stress tensor calculations (black arrows) and from Hillis and Reynolds [2003] (white arrows). The thick black arrows show the stress direction for the Pinjarra (PO) and Capricorn (CO) orogens as a whole, while the thinner black arrows show the stress directions for the subgroups of the Abrolhos group (Ab), Cape Range group (CR), Mirdalaya group (Mi), and Mount Clere group (MC) (see Table 6).

useful and consistent information of the orientation of the seismogenic crustal stress field. Such data has wide ranging applications in areas where in-situ data are sparse or absent.

[46] **Acknowledgments.** We thank the Australian Research Council, Woodside Petroleum, and Geoscience Australia for supporting this research through ARC Linkage grant LP0560955. We gratefully acknowledge the Australian National Seismic Imaging Resource for making the equipment available to this project, Geoscience Australia for managing the AU network, and Albuquerque Seismological Laboratory (USGS) for managing the IU Global Seismograph network for access to data recorded by the permanent network and made available through the services provided by IRIS. We thank Simon Johnson, Steve Sheppard, JGR associate editor Rodolfo Console and the two reviewers for very valuable and useful discussions and suggestions. We thank the pastoralists for the generous access to their properties and for their hospitality during our servicing trips.

## References

- Burbidge, D. R. (2004), Thin plate neotectonic models of the Australian plate, *J. Geophys. Res.*, *109*, B10405, doi:10.1029/2004JB003156.
- Clark, D. J., and M. Leonard (2003), Principal stress orientations from multiple focal-plane solutions: New insight into the Australia intraplate stress field, in *Evolution and Dynamics of the Australian Plate*, edited by R. R. Hillis and R. D. Müller, *Geol. Soc. of Am. Spec. Pap.*, *372*, 91–105.
- Clark, D. J., and K. McCue (2003), Australian paleoseismology: Towards a better basis for seismic hazard estimation, *Ann. Geophys.*, *46*(5), 1087–1105.
- Coblentz, D. D., S. Zhou, R. Hillis, R. M. Richardson, and M. Sandiford (1998), Topography boundary forces and the Indo-Australian intraplate stress field, *J. Geophys. Res.*, *103*(B1), 919–938.
- Dentith, M. C., and W. E. Featherstone (2003), Controls on intra-plate seismicity in southwestern Australia, *Tectonophysics*, *376*, 167–184.
- Eaton, J. W. (2002), *GNU Octave Manual*, Network Theory Limited, U. K.
- Fitzsimons, I. C. W. (2003), Proterozoic basement provinces of southern and southwestern Australia, and their correlation with Antarctica, in *Proterozoic East Gondwana: Supercontinent Assembly and Breakup*, edited by M. Yoshida, B. F. Windley, and S. Dasgupta, *Geol. Soc. Spec. Publ.*, *206*, 93–130.
- Gephart, J. W. (1990a), FMSI: A FORTRAN program for inverting fault/slickenside and earthquake focal mechanism data to obtain the regional stress tensor, *Comput. Geosci.*, *16*, 953–989.
- Gephart, J. W. (1990b), Stress and the direction of slip on fault planes, *Tectonics*, *9*(4), 845–858.
- Gephart, J. W., and D. W. Forsyth (1984), An improved method for determining the regional stress tensor using earthquake focal mechanism data: Application to the San Fernando earthquake sequence, *J. Geophys. Res.*, *89*(B11), 9305–9320.
- Hardebeck, J. L., and E. Hauksson (2001), Stress orientations obtained from earthquake focal mechanisms: What are appropriate uncertainty estimates?, *Bull. Seismol. Soc. Am.*, *91*(2), 250–262.
- Harris, L. B. (1994), Structural and tectonic synthesis for the Perth Basin, Western Australia, *J. Pet. Geol.*, *17*, 129–156.
- Herrmann, R. B., and C. J. Ammon (2007), *Computer Programs in Seismology: Surface Waves, Receiver Functions and Crustal Structure*, ver. 3.30, Saint Louis Univ., Saint Louis, Mo.
- Hillis, R. R., and S. D. Reynolds (2003), In situ stress field of Australia, in *Evolution and Dynamics of the Australian Plate*, edited by R. R. Hillis and R. D. Müller, *Geol. Soc. of Am. Spec. Pap.*, *372*, 49–58.
- Jaeger, J. C., and N. G. W. Cook (1979), *Fundamentals of Rock Mechanics*, 3rd ed., 593 pp., Chapman and Hall, London, U. K.
- Johnston, A. C., K. J. Coppersmith, L. R. Kanter, and C. A. Cornell (1994), The earthquakes of stable continental regions: Assessment of large earthquake potential, *Tech. Rep. TR-102261*, Electr. Power Res. Inst., Palo Alto, Calif.
- Kilb, D., and J. L. Hardebeck (2006), Fault parameter constraints using relocated earthquakes: A validation of first-motion focal-mechanism data, *Bull. Seismol. Soc. Am.*, *96*(3), 1140–1158.
- Lahr, J. C. (1999), Hypoellipse: A computer program for determining local earthquake hypocentral parameters, magnitude, and first-motion pattern, *U.S. Geol. Surv. Open-File Rep.* 99–23.
- Leonard, M. (2008), One hundred years of earthquake recording in Australia, *Bull. Seismol. Soc. Am.*, *98*(3), 1458–1470.
- Leonard, M., I. Ripper, and Y. Li (2002), Australian earthquake fault plane solutions, *Geosci. Australia Rec.*, *19*, 114 pp.

- Leonard, M., D. Robinson, T. Allen, J. Schneider, D. Clark, T. Dhu, and D. Burbidge (2007), Toward a better model of earthquake hazard in Australia, in *Continental Intraplate Earthquakes: Science, Hazard, and Policy Issues*, edited by S. Stein and S. Mazzotti, *Geol. Soc. of Am. Spec. Pap.*, 425, 263–283.
- Matur, S. P. (1974), Crustal structure in southwestern Australia from seismic and gravity data, *Tectonophysics*, 24, 151–182.
- Mazzotti, S. (2007), Geodynamic models for earthquake studies in intraplate North America, in *Continental Intraplate Earthquakes: Science, Hazard, and Policy Issues*, edited by S. Stein and S. Mazzotti, *Geol. Soc. of Am. Spec. Pap.*, 425, 17–33.
- McCue, K. (1990), Australia's largest earthquakes and Recent fault scarps, *J. Struct. Geol.*, 12, 761–766.
- Myers, J. S., and R. M. Hocking (1998), *Geological Map of Western Australia*, scale 1:2,500,000, Geol. Surv. of West. Aust.
- Myers, J. S., R. D. Shaw, and I. M. Tyler (1996), Tectonic evolution of Proterozoic Australia, *Tectonics*, 15(6), 1431–1446.
- Oppenheim, A. V., and R. Schafer (1999), *Discrete-Time Signal Processing, Prentice-Hall Signal Proc. Ser.*, 2nd ed., xxvi + 870 pp., Prentice-Hall, Upper Saddle River, N. J.
- Reasenber, P. A., and D. Oppenheimer (1985), FPFIT, FPLOT and FPPAGE: Fortran computer programs for calculating and displaying earthquake fault-plane solutions, *U.S. Geol. Surv., Open-File Rep.* 85–739.
- Revets, S. A. (2009), One-norm misfit statistics, *Geophys. Res. Lett.*, doi:10.1029/2009GL039808, in press.
- Reynolds, S. D., D. D. Coblenz, and R. R. Hillis (2002), Tectonic forces controlling the regional intraplate stress field in continental Australia: Results from new finite element modeling, *J. Geophys. Res.*, 107(B7), 2131, doi:10.1029/2001JB000408.
- Reynolds, S. D., D. D. Coblenz, and R. R. Hillis (2003), Influences of plate-boundary forces on the regional intraplate stress field of continental Australia, in *Evolution and Dynamics of the Australian Plate*, edited by R. R. Hillis and R. D. Müller, *Geol. Soc. of Am. Spec. Pap.*, 372, 59–70.
- Sandiford, M., and D. L. Egholm (2008), Enhanced intraplate seismicity along continental margins: Some causes and consequences, *Tectonophysics*, 364, 1–12.
- Scherbaum, F. (2001), *Of Poles and Zeros, Modern Approaches in Geophysics*, vol. 15, 2nd ed., xiii + 268 pp., Kluwer Acad., Dordrecht, Netherlands.
- Spassov, E. (1998), The stress field in Australia from composite fault plane solutions of the strongest earthquakes in the continent, *J. Seismol.*, 2, 173–178.
- Stein, S. (2007), Approaches to continental intraplate earthquake issues, in *Continental Intraplate Earthquakes: Science, Hazard, and Policy Issues*, edited by S. Stein and S. Mazzotti, *Geol. Soc. of Am. Spec. Pap.*, 425, 1–16.
- Stein, S., and S. Mazzotti (Eds.) (2007), *Continental Intraplate Earthquakes: Science, Hazard, and Policy Issues*, *Geol. Soc. of Am. Spec. Pap.*, 425.
- Tregoning, P. (2003), Is the Australian plate deforming? A space geodetic perspective, in *Evolution and Dynamics of the Australian Plate*, edited by R. R. Hillis and R. D. Müller, *Geol. Soc. of Am. Spec. Pap.*, 372, 41–48.
- Zizicas, G. A. (1955), Representation of three-dimensional stress distributions by Mohr circles, *J. Appl. Mech.*, 22, 273–274.

---

M. Keep and S. A. Revets, School of Earth and Environment, University of Western Australia, 35 Stirling Highway M004, Crawley, WA 6008, Australia. (myra.keep@uwa.edu.au; stefan.revets@uwa.edu.au)

B. L. N. Kennett, Research School of Earth Sciences, Australian National University, 61 Mills Road, Canberra, ACT 0200, Australia. (brian.kennett@anu.edu.au)